

# AIRS Deconvolution and Translation from the AIRS to CrIS IR Sounders

\*\*\*\* DRAFT \*\*\*\*

Howard E. Motteler  
L. Larrabee Strow

UMBC Atmospheric Spectroscopy Lab  
Joint Center for Earth Systems Technology

June 6, 2017

## 1 Introduction

Upwelling infrared radiation as measured by the AIRS [1] and CrIS [2, 6] sounders is a significant part of the long term climate record. We would like to treat this as a single data set and often want to compare radiances, for example in the analysis of simultaneous nadir overpasses (SNOs) for sounder calibration or validation. However the instruments have different spectral resolutions, channel response functions, and band spans. As a step in addressing this problem we consider the translation of channel radiances from AIRS to standard resolution CrIS.

Translation from AIRS to CrIS involves more than basic resampling. AIRS is a grating spectrometer with a distinct response function for each channel determined by the focal plane geometry, while CrIS is a Michelson interferometer with a sinc response function, after calibration and corrections. In section 2 we show how to take advantage of our detailed knowledge of the AIRS spectral response functions (SRFs) and their overlap to deconvolve channel radiances to a resolution-enhanced intermediate representation, typically a  $0.1\text{ cm}^{-1}$  grid, the approximate resolution of the tabulated AIRS SRFs.

This intermediate representation can then be reconvolved, for example to an idealized grating instrument with a generalized Gaussian response

function or to the CrIS user grid with a sinc basis. Section 3 gives details and validation tests for the AIRS to CrIS translation. In section ?? we consider alternate translations, including conventional interpolation and direct regression from AIRS to CrIS. Section 6 gives some applications and conclusions.

## 2 AIRS Deconvolution

The AIRS spectral response functions model channel response as a function of frequency and associate channels with nominal center frequencies. Each AIRS channel  $i$  has an associated spectral response function or SRF  $\sigma_i(v)$  such that the channel radiance  $c_i = \int \sigma_i(v)r(v) dv$ , where  $r$  is radiance at frequency  $v$ . The center or peak of  $\sigma_i$  is the nominal channel frequency.

Figure 1 shows typical AIRS SRFs from the low and high ends of the band. Note the significant overlap in the wings. This can allow for a deconvolution to recover resolution beyond that of the response functions considered individually. The SRFs are not necessarily symmetrical, especially at the high end of the band. The dashed line on top of the third SRF is a fit of a generalized Gaussian, which we consider in more detail later in this section. Figure 2 shows channel spacing and resolving power for the AIRS L1c channel set [?]. The variable channel spacing and resolving power are due to the modular structure of the focal plane. Although not entirely regular—that is, not a simple function of frequency—the L1c channel set is more regular than the L1b channel set from which it is derived, and we mainly consider the L1c set here.

Suppose we have  $n$  channels and a frequency grid  $\vec{v}$  of  $k$  points spanning the union of the domains of the functions  $\sigma_i$ . The grid step size for our applications is often  $0.0025 \text{ cm}^{-1}$ , the kcarta resolution [4]. Let  $S_k$  be an  $n \times k$  array such that  $s_{i,j} = \sigma_i(v_j)/w_i$ , where  $w_i = \sum_j \sigma_i(v_j)$ , that is where row  $i$  is  $\sigma_i(v)$  tabulated at the grid  $\vec{v}$  and normalized so the row sum is 1. If the channel centers are in increasing order  $S_k$  is banded, and if they are not too close (as is the case for a few of the L1b channels) the rows are linearly independent.  $S_k$  is a linear transform whose domain is radiance at the grid  $\vec{v}$  and whose range is channel radiances. If  $r$  is radiance at the grid  $\vec{v}$ , then  $c = S_k r$  gives a good approximation of the channel radiances  $c_i = \int \sigma_i(v)r(v) dv$ . In practice this is how we convolve kcarta or other high resolution calculated radiances to get AIRS channel radiances, for example for reference truth or “true AIRS” for the tests shown here.

For the AIRS to CrIS and other translations we are mainly interested

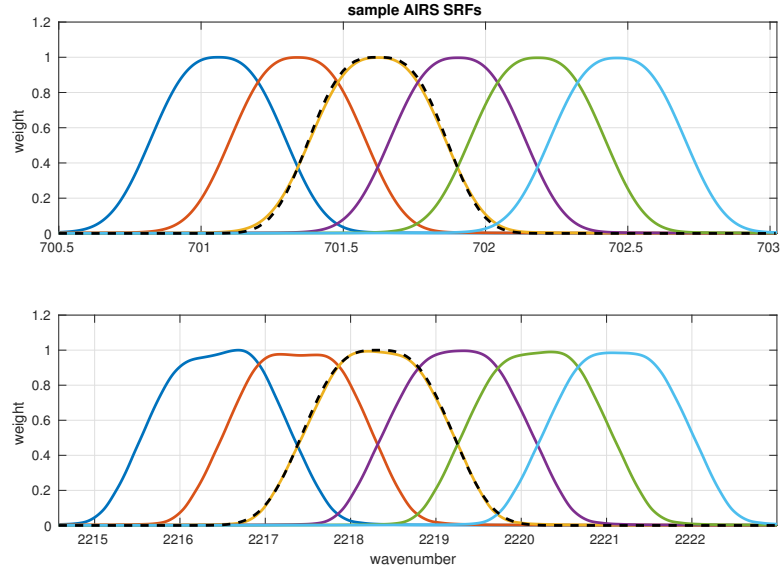


Figure 1: sample AIRS spectral response functions from the low and high ends of the band. The dashed line is a generalized Gaussian function.

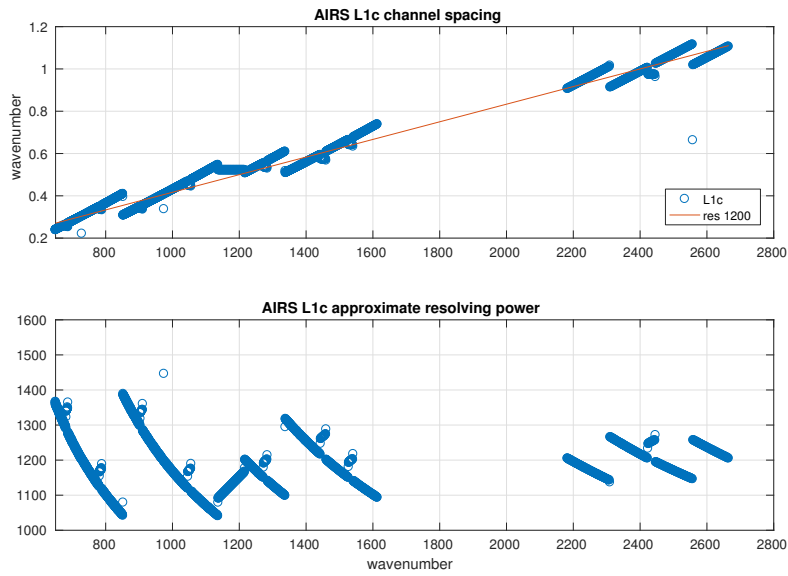


Figure 2: AIRS L1c channel spacing and derived resolving power.

in the transform  $S_b$  for SRFs at an intermediate resolution, typically  $0.1 \text{ cm}^{-1}$ . This is the approximate resolution of the SRF measurements and convenient for reconvolution to the CrIS user grid. So let  $\vec{v}_b = v_1, v_2, \dots, v_m$  be a  $0.1 \text{ cm}^{-1}$  grid spanning the domains of the functions  $\sigma_i$ . Similar to  $S_k$ , let  $S_b$  be an  $n \times m$  array where row  $i$  is  $\sigma_i(v)$  tabulated at the  $\vec{v}_b$  grid, with rows normalized to 1. If  $r$  is radiance at the  $\vec{v}_b$  grid, then  $c = S_b r$  is still a reasonable approximation of  $\int \sigma_i(v) r(v) dv$ .

For our application we want to start with  $c$  and find  $r$ , that is to deconvolve  $c$  by solving  $S_b r = c$  for  $r$ . Since  $m < k$ , the system is underdetermined, but we can take  $r$  as  $r_0 = S_b^{-1} c$  where  $S_b^{-1}$  is the Moore-Penrose pseudoinverse [?] of  $S_b$ . This has the key property of finding  $r_0$  such that  $\|r_0\|_2 \leq \|r_j\|_2$  for all  $r_j$  satisfying  $S_b r_j = c$ . The condition number for  $S_b$  built from the L1c channels is  $\|S_b\|_2 \|S_b^{-1}\|_2 = 115$ , which is acceptable.

Although our main goal is to reconvolve the  $0.1 \text{ cm}^{-1}$  intermediate representation to the CrIS or other user grids, we first compare the deconvolved radiances with reference truth from a direct convolution to intermediate grid. The choice of response functions for this direct convolution is not obvious, since the deconvolution is undoing—at least to some extent—the effects of the AIRS SRF convolutions. We use a generalized Gaussian of the form

$$w = \exp \left( - \left( \frac{(x - v_0)^2}{2c^2} \right)^{1.5} \right)$$

where  $c = \text{FWHM}/2.355$  and  $v_0$  is the desired channel center. The exponent 1.5 was chosen to give an approximate match to AIRS SRFs with the same FWHM and channel centers, though without the fine structure and variation of the latter. Figure 1 shows two such functions paired with AIRS SRFs with the same FWHM and centers. We used this function for the  $0.1 \text{ cm}^{-1}$  intermediate grid with  $\text{FWHM} = v_i/2000$  where  $v_i$  are the grid frequencies. This represents a hypothetical grating spectrometer with a resolving power of 2000, oversampled to the  $0.1 \text{ cm}^{-1}$  grid.

The AIRS deconvolution gives a modest resolution enhancement, at the cost of added artifacts and noise. Figure 3 shows details of kcarta, direct convolution to the  $0.1 \text{ cm}^{-1}$  grid (“gauss”), deconvolution, and AIRS spectra for fitting profile 1 [3, 5]. In the first subplot we see the deconvolution is capturing some of the fine structure in the kcarta data that is present in the direct convolution but not in the AIRS data. In the second subplot we see the deconvolution (and direct convolution) resolving a pair of close lines that are not resolved at the AIRS L1c resolution. But we also see some ringing that is not present in the direct convolution. Figure 4 shows the

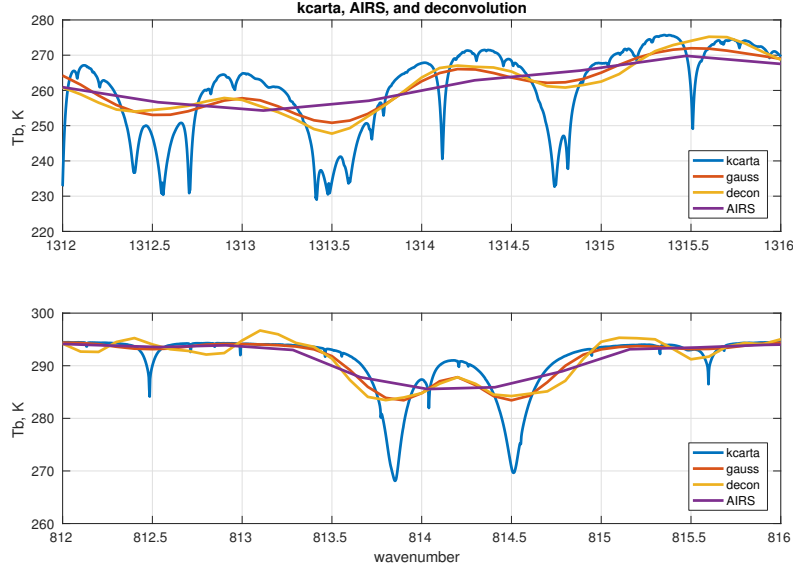


Figure 3: details from fitting profile 1 for kcarta, direct convolution to the  $0.1 \text{ cm}^{-1}$  grid ("gauss"), deconvolved AIRS, and true AIRS.

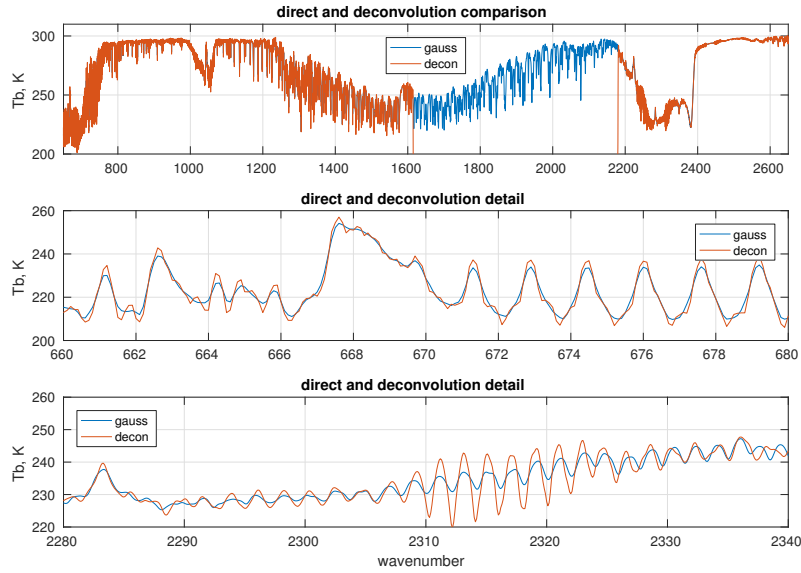


Figure 4: spectra from fitting profile 1 for direct convolution to the  $0.1 \text{ cm}^{-1}$  grid ("gauss") and deconvolved AIRS

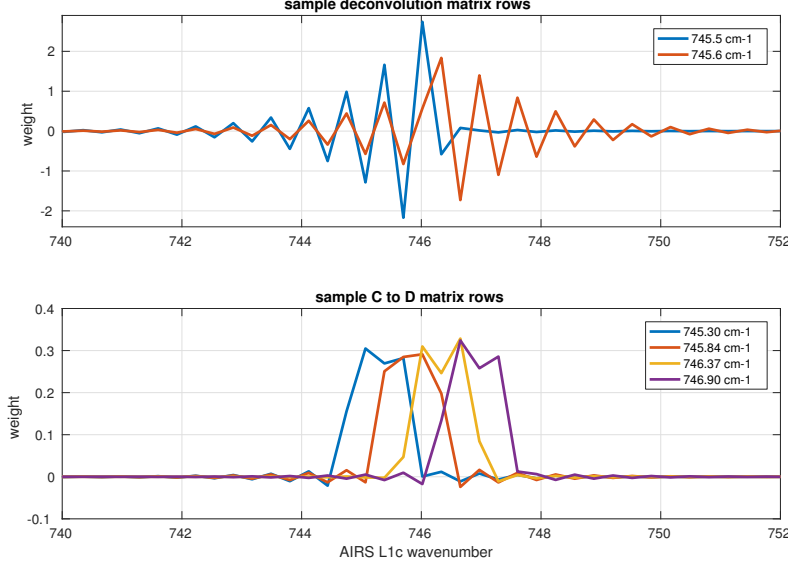


Figure 5: sample adjacent rows for the deconvolution and L1c to L1d transforms

full spectra from fitting profile 1, along with sample details from the low and high ends of the band, for the deconvolution and direct convolution to the intermediate grid. In the details we see some overshoot and ringing in the deconvolution. But we do not propose using the deconvolved radiances directly, they are an intermediate step in reconvolution to a lower resolution.

Figure 5 shows a pair of typical adjacent rows of the deconvolution matrix  $S_b^{-1}$  in the first subplot. Row  $i$  of  $S_b^{-1}$  is the weights applied to L1c channel radiances to synthesize the deconvolved radiance  $r_i$  at the intermediate grid frequency  $v_i$ . The oscillation simply means we are taking the closest AIRS channel, subtracting weighted values for channels  $\pm 1$  step away, adding weighted values for channels  $\pm 2$  steps away, and so on, with the weights decreasing quickly as we move away from  $v_i$ , with eight to ten L1c channels making a significant contribution to each deconvolution grid point.

The second subplot shows four adjacent rows of the matrix  $S_d \cdot S_b^{-1}$ , which takes L1c to L1d channel radiances. (The L1d radiances are discussed in a later section; here they are of interest mainly as a typical reconvolution.) Both matrices are banded but the bands are narrower in the second, with three to five L1c channels contributing significantly to each L1d channel. The range of influence is significant since for example we may want to see which L1d channels are derived in part from the subset of synthetic L1c

channels.

### 3 AIRS to CrIS translation

Given deconvolution to the  $0.1 \text{ cm}^{-1}$  intermediate grid, reconvolution to the CrIS user grid is straightforward. For CrIS standard resolution the channel spacing is  $0.625 \text{ cm}^{-1}$  for the LW,  $1.25 \text{ cm}^{-1}$  for the MW, and  $2.5 \text{ cm}^{-1}$  for the SW bands. For each CrIS band, we (1) find the AIRS and CrIS band intersection, (2) apply a bandpass filter to the deconvolved AIRS radiances restricting them to the intersection, with a rolloff outside the intersection, and (3) reconvolve the filtered spectra to the CrIS user grid with a zero-filled double Fourier transform.

Translations are validated by comparison with calculated reference truth. We start with a set of atmospheric profiles and calculate upwelling radiance at a  $0.0025 \text{ cm}^{-1}$  grid with kcarta [4] over a band spanning the domains of the AIRS and CrIS response functions. “True AIRS” is calculated by convolving the kcarta radiances with AIRS SRFs and “true CrIS” by convolving kcarta radiances to a sinc basis at the CrIS user-grid specifications. True AIRS is then translated to CrIS to get “AIRS CrIS”, and this is compared with true CrIS. Figure 6 shows sample spectra for true AIRS, deconvolved AIRS, true CrIS and AIRS CrIS. This approach assumes perfect knowledge of the AIRS and CrIS instrument response functions and so gives only a lower bound on residuals. But in practice we know the response functions very well [?, ?].

Results are validated with a set of 49 fitting profiles spanning a wide range of clear atmospheric conditions, initially chosen for testing radiative transfer codes [3, 5]. The 49 profile set is largely uncorrelated, in the sense that reducing the reconstruction RMS residual to 0.02 K for radiances calculated from the profiles requires 48 left-singular vectors. For statistical correction and direct regression (discussed later) we also use a set of 7377 radiances calculated from mostly cloudy AIRS profiles spanning several consecutive days, as the dependent set. This set is moderately correlated; reducing the reconstruction RMS residual to 0.02 K for radiances calculated from the profiles requires 260 left-singular vectors. For all cases considered here the 49 profile set gives a stricter test than splitting the 7377 profile set into dependent and independent sets as residuals with the 49-profile set are consistently larger.

Figures 7, 8, and 9 show the mean and standard deviation of true CrIS minus AIRS CrIS for the 49 fitting profiles, with and without Hamming apodization, for each of the CrIS bands. Figure 10 summarizes these re-

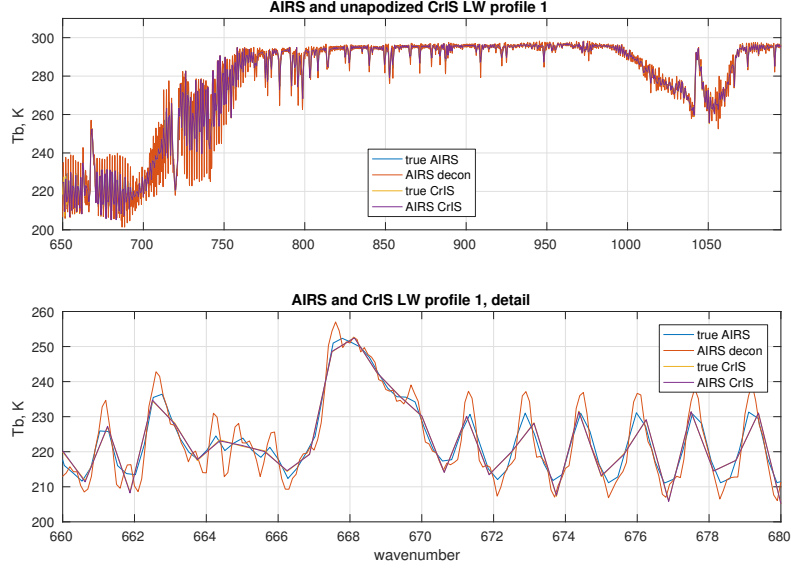


Figure 6: true AIRS, deconvolved AIRS, true CrIS, and AIRS CrIS

sults for Hamming apodized radiances. The residual has a high frequency component with a period of 2 channel steps that is significantly reduced by the apodization. The constant or DC bias (the mean of the residuals over frequency) is very close to zero for the apodized residuals.

There is some regularity in the residual, including an oscillation with period two channel steps. Up to this point there is no statistical component to our translation, beyond finding a good test set for validation. We feel it is important to be clear about any steps that require statistical fitting. That said, a simple linear correction can give a significantly further reduction in the validation residual. For the statistical tests we use the set of 7377 mostly cloudy AIRS profiles as the dependent set and the 49 profile set the independent or test set.

We compare three such corrections. These are done with a separate regression for each CrIS channel, and so introduce no cross-correlations. Let  $t_i^{\text{TC}}$  be true CrIS and  $t_i^{\text{AC}}$  AIRS to CrIS brightness temperatures for CrIS channel  $i$ , both from the dependent set. For the bias test we subtract the mean residual from the dependent set. For the linear test we find  $a_i$  and  $b_i$  to minimize  $\|a_i t_i^{\text{AC}} + b_i - t_i^{\text{TC}}\|_2$  and for the quadratic test weights  $c_i$ ,  $a_i$  and  $b_i$  to minimize  $\|c_i (t_i^{\text{AC}})^2 + a_i t_i^{\text{AC}} + b_i - t_i^{\text{TC}}\|_2$ .

Figure 11 is a comparison of bias, linear, and quadratic corrections for



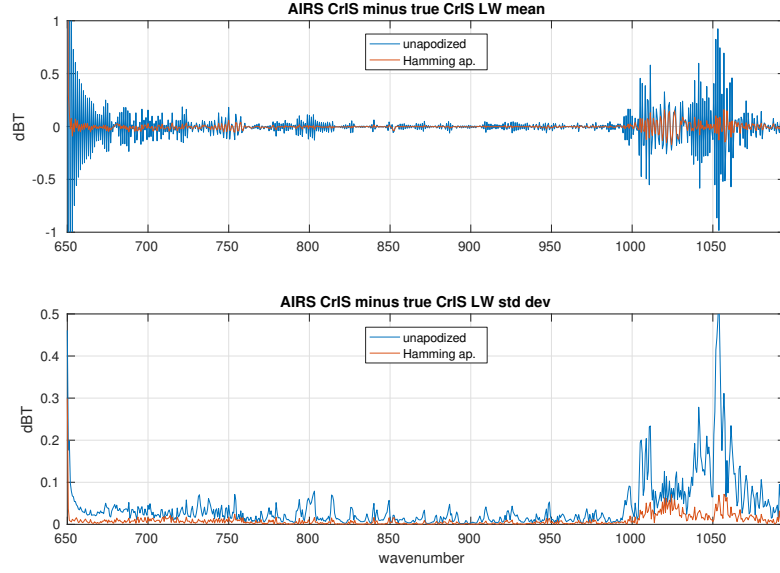


Figure 7: Mean and standard deviation of unapodized and Hamming apodized AIRS CrIS minus true CrIS, for the CrIS LW band

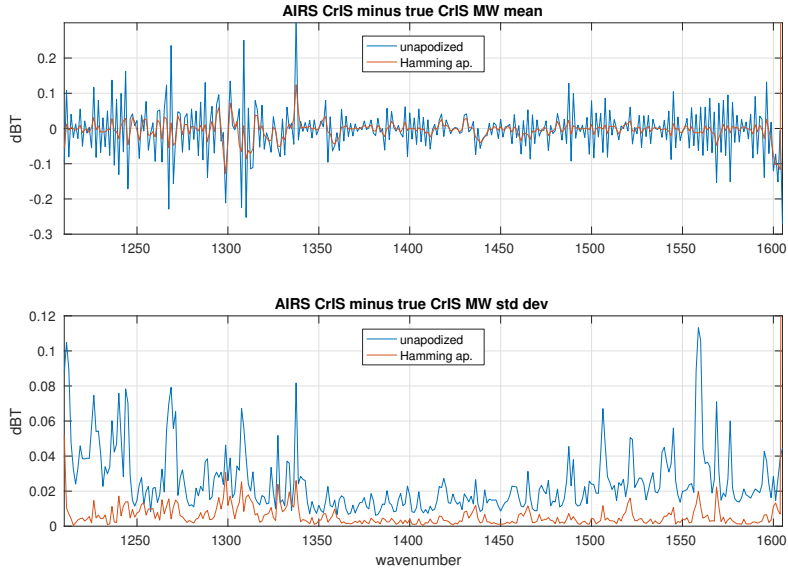


Figure 8: Mean and standard deviation of unapodized and Hamming apodized AIRS CrIS minus true CrIS, for the CrIS MW band

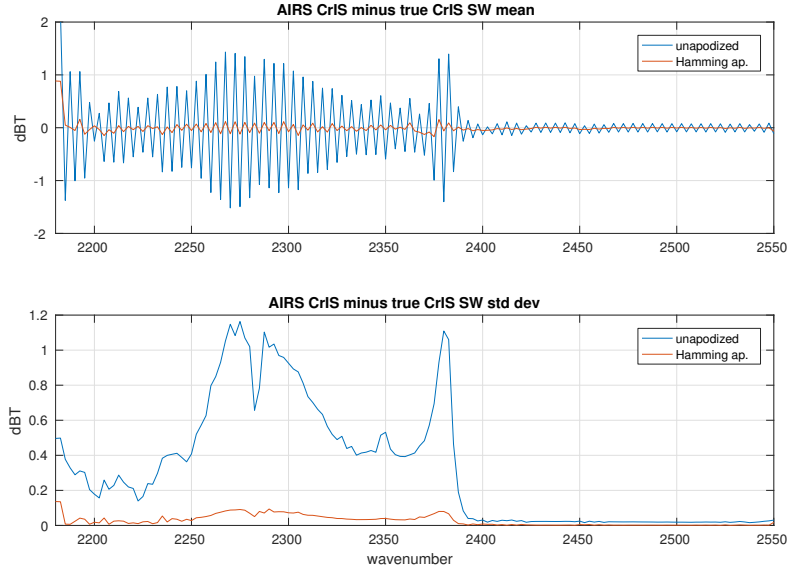


Figure 9: Mean and standard deviation of unapodized and Hamming apodized AIRS CrIS minus true CrIS, for the CrIS SW band

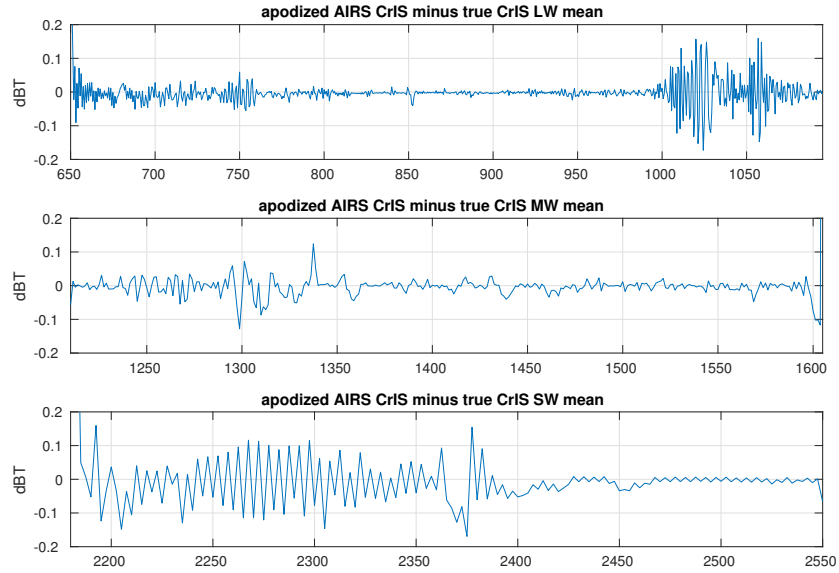


Figure 10: Mean of apodized residuals for all three CrIS bands

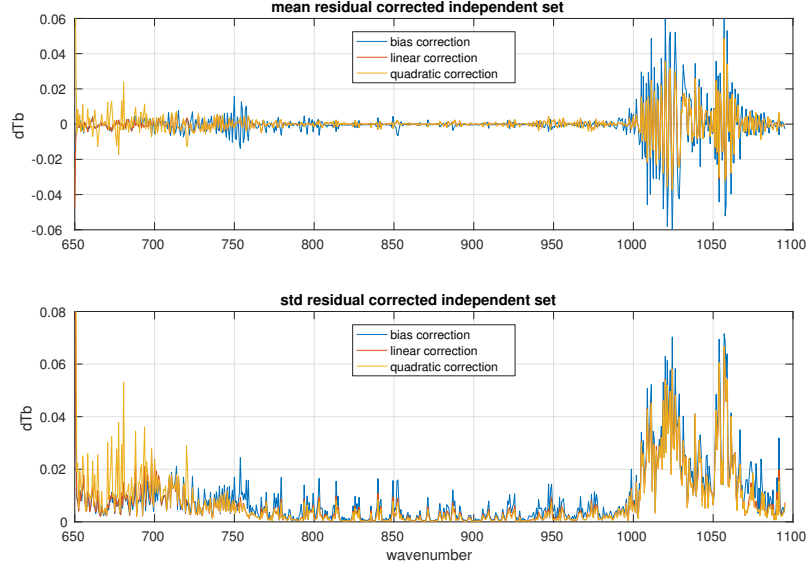


Figure 11: Mean and standard deviation of LW corrected apodized residuals

the LW band. The linear and quadratic corrections are nearly identical, and the quadratic coefficient is very close to zero. Figure 12 shows the weights for the linear fits from figure 11. The  $a$  weight is very close to 1 and the  $b$  weight to the bias. Figures 13 and 14 show the linear correction giving a similar improvement in the MW and a small improvement in the SW, where the quadratic correction is noticeably worse. Figure 15 summarized results for the linear correction, pairing these with the apodized uncorrected residuals.

We can give a reasonable estimate of noise equivalent differential radiance (NEdN) as follows. We start with AIRS L1c and CrIS NEdN estimates. The L1c spec is the average over a day (4 Dec 2016) of NEdN values from the L1c granules, with gaps for the synthetic channels filled in by interpolation. The CrIS values are from a single CCAST ?? granule. The CrIS values are quite stable over time and consistent with other CrIS NEdN estimates. Results are summarized in figure 16.

Noise with a normal distribution at the AIRS spec is added to true AIRS and then measured. The measured AIRS noise is the “test” line in the plot. This is very close to the spec and so serves as a sanity check for our methods. True AIRS with added noise is then translated to CrIS and the noise of the translation is measured. This is the AIRS to CrIS line in the plots. The

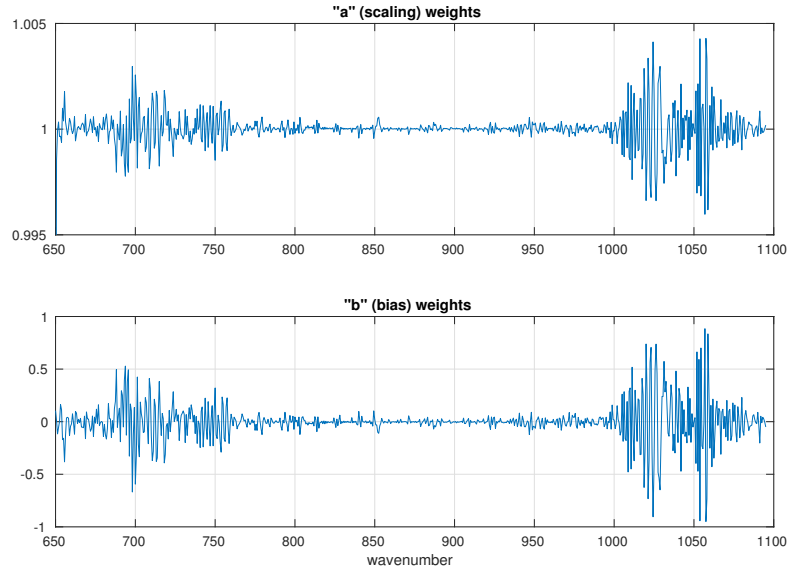


Figure 12: LW  $a$  and  $b$  weights for the linear correction  $ax + b$

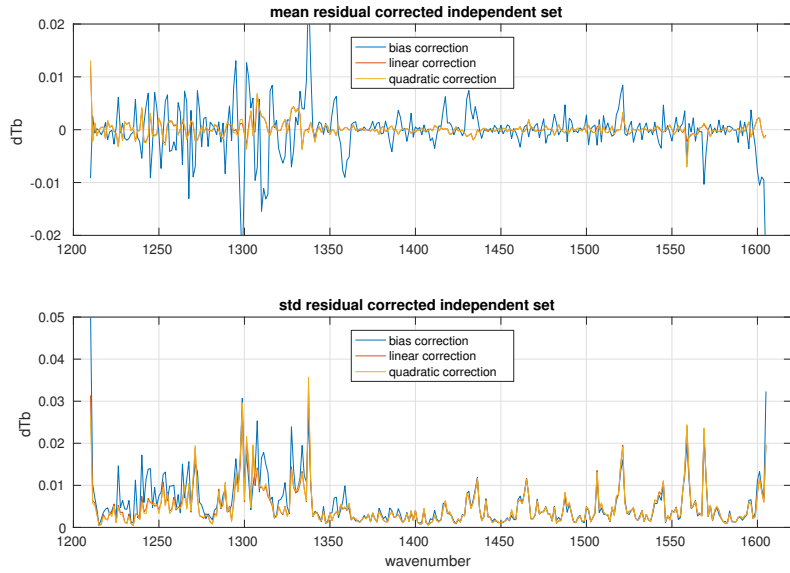


Figure 13: Mean and standard deviation of MW corrected apodized residuals.

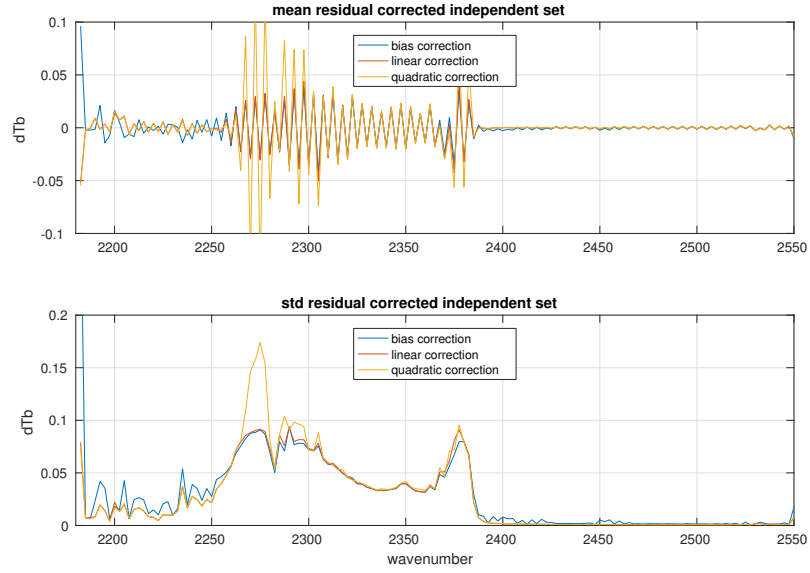


Figure 14: Mean and standard deviation of SW corrected apodized residuals.

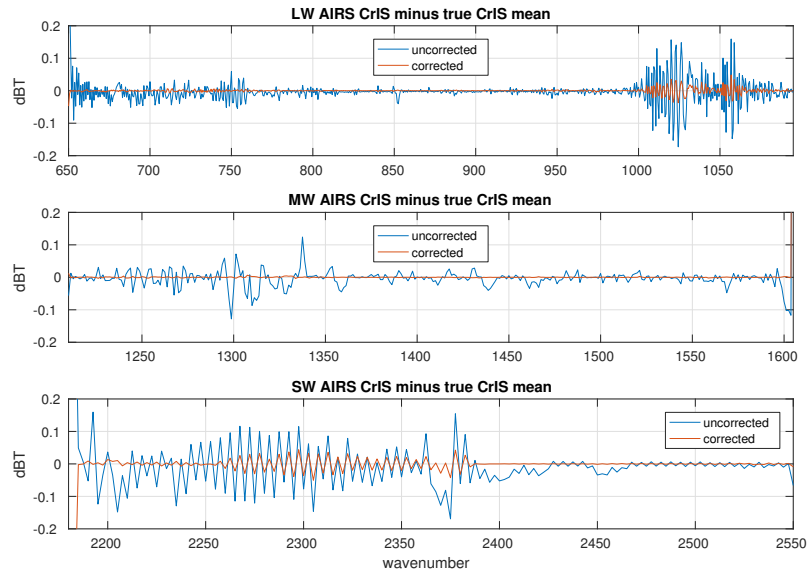


Figure 15: Mean corrected apodized residuals for all three bands.

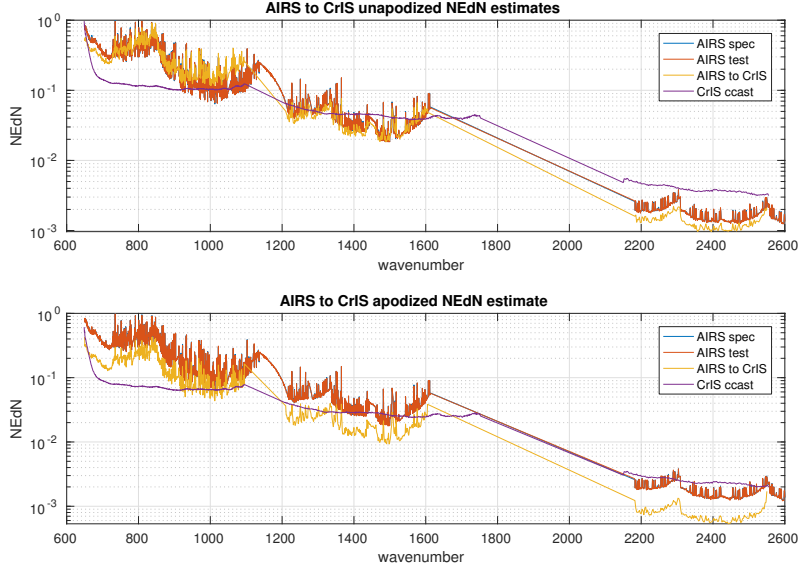


Figure 16: AIRS to CrIS unapodized and apodized NEdN estimates

unapodized translation tracks the AIRS noise spec fairly closely in the LW and MW, and is a little less in the SW. Unapodized AIRS to CrIS noise is a little higher than true CrIS noise in the LW, a little less in the MW, and significantly less in the SW, and this relationship is unchanged with apodization.

Translation with deconvolution works significantly better than interpolation for the AIRS to CrIS translation. We consider two cases. For the first, start with true AIRS and interpolate radiances directly to the CrIS user grid with a cubic spline. For the second, interpolate true AIRS to the  $0.1 \text{ cm}^{-1}$  intermediate grid with a cubic spline and then convolve this to the use CrIS user grid. Figure 17 shows interpolated CrIS minus true CrIS for the LW band, without apodization. The two-step interpolation works a little better than the simple spline, but both residuals are significantly larger than for the translation with deconvolution. Results for the MW are similar, while the unapodized comparison is less clear for the SW. With Hamming apodization, the residuals with deconvolution are significantly less than interpolation for all three bands.

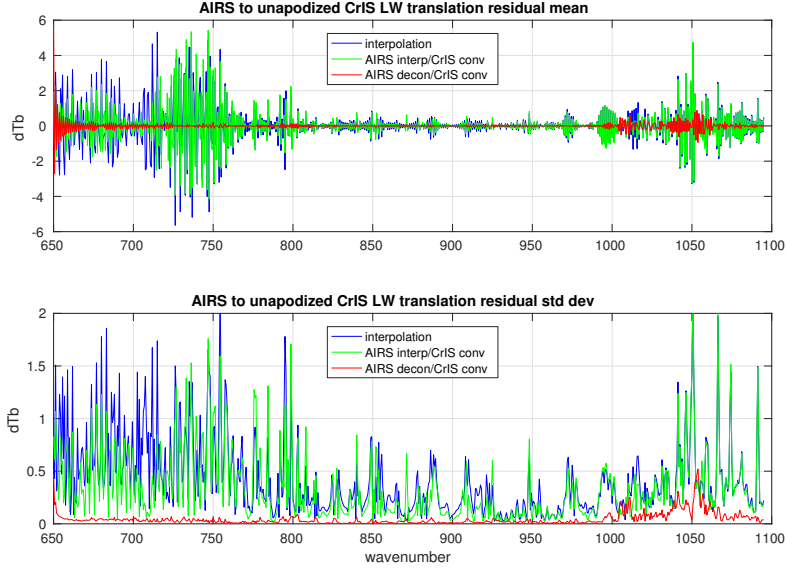


Figure 17: spline interpolation, interpolation with convolution, and deconvolution with convolution for the CrIS LW band

## 4 Translation to an idealized grating instrument

The AIRS deconvolution can be used for other translations. We consider reconvolution to idealized grating instruments with resolving power of 1200 and 700. Define an AIRS L1d basis with the generalized Gaussian response function above, with  $\text{FWHM} = v/\text{resolving power}$  and  $dv = \text{FWHM}/2$ , and with the  $dv$ -spaced channel steps starting at  $v_0$ . In contrast with the regular spacing used for the  $0.1 \text{ cm}^{-1}$  intermediate grid, this is not oversampled.

Figure 18 shows residuals for reconvolution to an L1d basis with resolving power of 1200, the nominal AIRS resolution and figure 19 shows residuals for a resolving power of 700, half the best AIRS resolving power of 1400 in the LW. Note the different x-axes in the two figures. The uncorrected residuals are for the deconvolution/reconvolution transform “L1C to D” minus “true L1D”, Resolution is lost in shifting channel centers to a single regular function of frequency. The L1d residuals depend in part on the starting channel, and so on how the SRF peaks line up with the L1c set. The residuals above are the result of a rough fit for  $v_0$ . For a resolving power of 1200 this gave  $v_0$  equal to the first L1c channel, while for 700 it was the first L1c channel plus  $0.2 \text{ cm}^{-1}$ . As with the AIRS to CrIS translation, residuals are reduced significantly with a linear correction.

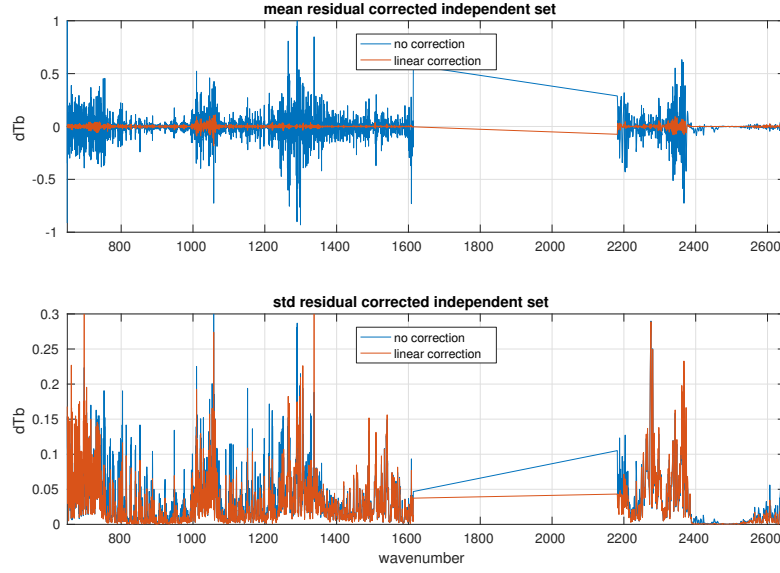


Figure 18: mean and standard deviation over the 49 fitting profiles for the L1c to L1d translation minus true L1d for a resolving power of 1200

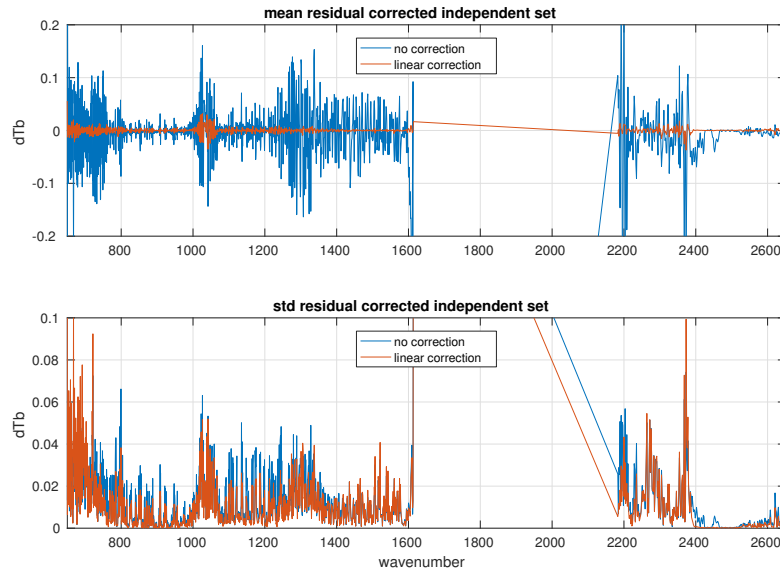


Figure 19: mean and standard deviation over the 49 fitting profiles for the L1c to L1d translation minus true L1d for a resolving power of 1200



As with the AIRS to CrIS translation, deconvolution is significantly better than interpolation for the L1c to L1d translation. We consider two cases. For the first, start with true L1c and interpolate radiances directly to the L1d grid with a cubic spline. For the second, interpolate true L1c to the  $0.1 \text{ cm}^{-1}$  intermediate grid with a cubic spline and convolve this to the L1d channel set. Figure 20 shows interpolated L1d minus true L1d. The two-step interpolation works a little better than the simple spline, but is still much larger than the residual for translation with deconvolution.

The L1c to L1d translation can be represented as a single linear transform  $S_d \cdot S_c^{-1}$ , where  $S_c$  and  $S_d$  are the transforms taking the intermediate grid to L1c and L1d channels and  $S_c^{-1}$  the pseudo-inverse of  $S_c$ , that is, the deconvolution transform. We can get such a transform in other ways, for example by regression to find  $X$  that minimizes the residual  $\|Xr_c - r_d\|_2$  for L1c and L1d radiance sets  $r_c$  and  $r_d$ . If  $r_c$  and  $r_d$  are  $m$  and  $n$  by  $k$  matrices, then if  $k \leq m$  we can simply solve for  $X$ . If  $k < m$  the system is underdetermined; in this case the residual is zero but extrapolation behavior is typically poor. If  $k > m$  we can find  $X$  by regression, and extrapolation behavior can be quite good if we regress against large sets of representative data. In practice this seems to work very well, at least for minimizing both dependent and independent set residuals. But in contrast with the sharply banded composite transform  $S_d \cdot S_c^{-1}$  the resulting transform is full of unexpected correlations and so may not be suitable for applications where we want to trace channel dependencies in the translation.

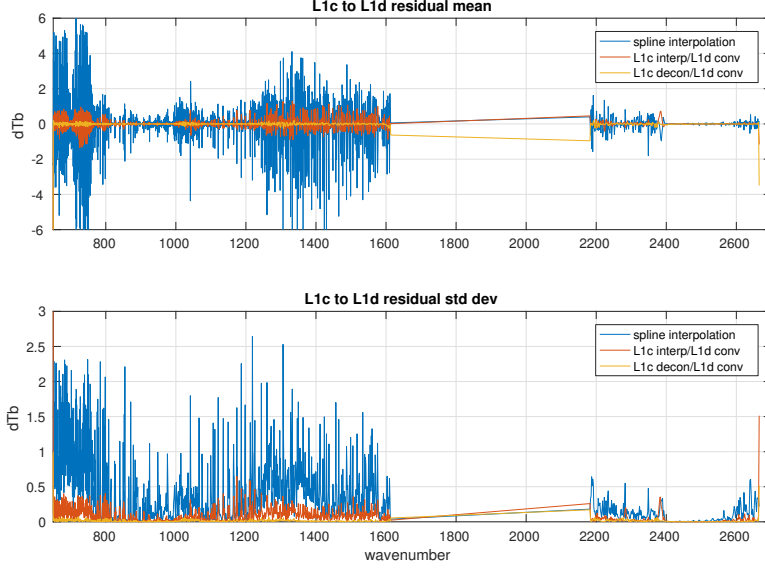


Figure 20: spline interpolation, interpolation with convolution, and deconvolution with convolution for the AIRS L1c to L1d translation with  $\nu_0 = 649.822 \text{ cm}^{-1}$  and a resolving power of 700

## 5 Direct regression

The L1c to L1d translation can be represented as a single linear transform  $S_d \cdot S_c^{-1}$ , where  $S_c$  and  $S_d$  are the transforms taking the intermediate grid to L1c and L1d channels and  $S_c^{-1}$  the pseudo-inverse of  $S_c$ , that is, the deconvolution transform. We can get such a transform in other ways, for example by regression to find  $X$  that minimizes the residual  $\|Xr_c - r_d\|_2$  for L1c and L1d radiance sets  $r_c$  and  $r_d$ . If  $r_c$  and  $r_d$  are  $m$  and  $n$  by  $k$  matrices, then if  $k \leq m$  we can simply solve for  $X$ . If  $k < m$  the system is underdetermined; in this case the residual is zero but extrapolation behavior is typically poor. If  $k > m$  we can find  $X$  by regression, and extrapolation behavior can be quite good if we regress against large sets of representative data. In practice this seems to work very well, at least for minimizing both dependent and independent set residuals. But in contrast with the sharply banded composite transform  $S_d \cdot S_c^{-1}$  the resulting transform is full of unexpected correlations and so may not be suitable for applications where we want to trace channel dependencies in the translation.

## 6 Applications and conclusions

### References

- [1] H. H. Aumann, M. T. Chahine, C. Gautier, M. D. Goldberg, E. Kalnay, L. M. McMillin, H. Revercomb, P. W. Rosenkranz, W. L. Smith, D. H. Staelin, L. L. Strow, and J. Susskind. AIRS/AMSU/HSB on the aqua mission: design, science objectives, data products, and processing systems. *IEEE Transactions on Geoscience and Remote Sensing*, 41:253–264, Feb. 2003.
- [2] Y. Han, H. Revercomb, M. Crompt, D. Gu, D. Johnson, D. Mooney, D. Scott, L. Strow, G. Bingham, L. Borg, Y. Chen, D. DeSlover, M. Esplin, D. Hagan, X. Jin, R. Knuteson, H. Motteler, J. Predina, L. Suwinski, J. Taylor, D. Tobin, D. Tremblay, C. Wang, L. Wang, L. Wang, and V. Zavyalov. Suomi NPP CrIS measurements, sensor data record algorithm, calibration and validation activities, and record data quality. *Journal of Geophysical Research (Atmospheres)*, 118:12734, Nov. 2013.
- [3] L. Strow, S. Hannon, S. De Souza-Machado, H. Motteler, and D. Tobin. An overview of the airs radiative transfer model. *Geoscience and Remote Sensing, IEEE Transactions on*, 41(2):303–313, Feb 2003.
- [4] L. Strow, H. E. Motteler, R. G. Benson, S. E. Hannon, and S. D. Souza-Machado. Fast computation of monochromatic infrared atmospheric transmittances using compressed look-up tables. *Journal of Quantitative Spectroscopy and Radiative Transfer*, 59(35):481 – 493, 1998. Atmospheric Spectroscopy Applications 96.
- [5] L. L. Strow, S. E. Hannon, S. De-Souza Machado, H. E. Motteler, and D. C. Tobin. Validation of the atmospheric infrared sounder radiative transfer algorithm. *Journal of Geophysical Research: Atmospheres*, 111(D9), 2006. D09S06.
- [6] L. L. Strow, H. Motteler, D. Tobin, H. Revercomb, S. Hannon, H. Buijs, J. Predina, L. Suwinski, and R. Glumb. Spectral calibration and validation of the Cross-track Infrared Sounder on the Suomi NPP satellite. *Journal of Geophysical Research (Atmospheres)*, 118:12486, Nov. 2013.